

# Cation– $\pi$ and $\pi$ – $\pi$ Interactions in Aqueous Solution Studied Using Polarizable Potential Models

Esam A. Orabi<sup>†</sup> and Guillaume Lamoureux\*

Department of Chemistry and Biochemistry and Centre for Research in Molecular Modeling, Concordia University, Montréal, Québec H4B 1R6, Canada

**ABSTRACT:** Polarizable potential models for the interaction of  $\text{Li}^+$ ,  $\text{Na}^+$ ,  $\text{K}^+$ , and  $\text{NH}_4^+$  ions with benzene are parametrized based on ab initio quantum mechanical calculations. The models reproduce the ab initio complexation energies and potential energy surfaces of the cation– $\pi$  dimers. They also reproduce the cooperative behavior of “stacked”, cation– $\pi$ – $\pi$  trimers and the anticooperative behavior of “sandwiched”,  $\pi$ –cation– $\pi$  trimers. The  $\text{NH}_4^+$  model is calibrated to reproduce the energy of the  $\text{NH}_4^+$ – $\text{H}_2\text{O}$  dimer and yields correct free energy of hydration and hydration structure without further adjustments. The models are used to investigate cation– $\pi$  interactions in aqueous solution by calculating the potential of mean force between each of the four cations and a benzene molecule and by analyzing the organization of the solvent as a function of the cation–benzene separation. The results show that  $\text{Li}^+$  and  $\text{Na}^+$  ions are preferentially solvated by water and do not associate with benzene, while  $\text{K}^+$  and  $\text{NH}_4^+$  ions bind benzene with 1.2 and 1.4 kcal/mol affinities, respectively. Molecular dynamics simulations of  $\text{NH}_4^+$  and of  $\text{K}^+$  in presence of two benzene molecules in water show that cation– $\pi$  and  $\pi$ – $\pi$  affinities are mutually enhanced compared to the pairwise affinities, confirming that the cooperativity of cation– $\pi$  and  $\pi$ – $\pi$  interactions persists in aqueous solution.

## 1. INTRODUCTION

Cation– $\pi$  interactions are noncovalent interactions between positively charged ions and the  $\pi$  electrons of aliphatic or aromatic compounds.<sup>1–5</sup> Such pairings of cations and  $\pi$  systems have been the subject of multiple experimental<sup>6–14</sup> and computational<sup>2–5,15–25</sup> studies. Experimental studies have shown that cation– $\pi$  interactions in the gas phase are competitive with some of the strongest noncovalent interactions.<sup>6,7,10–12</sup> Analysis of high-resolution structures in the Protein Data Bank<sup>26</sup> shows that cation– $\pi$  interactions are commonly found in proteins<sup>5,27</sup> and at protein–protein<sup>28</sup> and protein–DNA interfaces.<sup>29,30</sup> Cation– $\pi$  interactions contribute to protein stability,<sup>31,32</sup> protein–ligand interactions,<sup>1,33</sup> and to molecular recognition in general.<sup>34</sup>

Quantum mechanical (QM) calculations on cation– $\pi$  complexes correlate strongly with experimental gas phase data.<sup>2–5,9–12,14–25</sup> For instance, binding enthalpies of alkali metal ions with benzene calculated at state-of-the-art levels of theory have shown good agreement with experimental values.<sup>17</sup> QM calculations—and molecular mechanics models that accurately reproduce QM-calculated properties—thus serve as a convenient tool for studying and understanding cation– $\pi$  interactions. In particular, it has been shown that the dominant contributions to cation– $\pi$  interactions are electrostatics and polarization: charge–quadrupole and charge–induced dipole, mainly.<sup>1,2,35</sup> Other forces, such as dispersion and charge transfer, are much weaker. Electronic polarization is a determining factor, due to the strong electric field produced by the cation.<sup>15,16,18,22</sup>

Cation– $\pi$  interactions usually out-compete cation–water interactions in the gas phase. For example the enthalpy of formation of  $\text{K}^+$ –benzene complex in gas phase is –19.2 kcal/mol, compared to –17.9 kcal/mol for  $\text{K}^+$ – $\text{H}_2\text{O}$ .<sup>36</sup> Cation– $\pi$

interactions are weaker in solution than in gas phase,<sup>19</sup> due to the charge screening effect of the solvent and the high availability of water. Nevertheless, their existence in aqueous solution has been computationally<sup>37–39</sup> and experimentally<sup>8,13</sup> confirmed. While the computational and experimental literature on cation– $\pi$  interactions in the gas phase is abundant, studies of the interactions in water are few, and further work is required for a detailed understanding of their stability in solution.

Computational studies of cation– $\pi_2$  complexes in which  $\pi$  systems are arranged in a stacked geometry<sup>21,25</sup> show that cation– $\pi$  and  $\pi$ – $\pi$  interactions are cooperative: The presence of one interaction strengthens the other and results in a net increase of the complex stabilization energy.<sup>25</sup> It is however not clear how such cooperativity in gas phase translates in aqueous solution, where cation– $\pi$  interactions are competing with cation–water interactions and where  $\pi$ – $\pi$  interactions are stabilized by the hydrophobic effect. These are likely important considerations for the binding of cationic moieties to proteins.

Owing to the biological importance of cation– $\pi$  interactions and the computational prohibition of QM calculations on these systems, computationally inexpensive yet accurate molecular models for these interactions are crucial. Since electronic polarization represents an important contribution to cation– $\pi$  interactions,<sup>15,35</sup> polarizable potential models are required.

In this work, we parametrize polarizable empirical force fields for the interaction of  $\text{Li}^+$ ,  $\text{Na}^+$ ,  $\text{K}^+$ , and  $\text{NH}_4^+$  with benzene as well as for the interaction of  $\text{NH}_4^+$  with water. Electronic polarization in the systems is described using classical Drude oscillators.<sup>40–42</sup> We apply these models to investigate cation–benzene

Received: August 15, 2011

Published: November 09, 2011

interactions in water and their interplay with benzene–benzene interactions. The  $\text{NH}_4^+–\text{H}_2\text{O}$  interaction model is validated by calculating the free energy of hydration and hydration structure of the ion.

We perform ab initio calculations (geometry optimizations and potential energy scans) on the four cation–benzene complexes as well as on the  $\text{NH}_4^+–\text{H}_2\text{O}$  complex. The calculated ab initio properties are then used to parametrize the polarizable potential models. Molecular dynamics (MD) simulations of  $\text{M}^+–\text{benzene}$  (where  $\text{M}^+$  is  $\text{Li}^+$ ,  $\text{Na}^+$ ,  $\text{K}^+$ , or  $\text{NH}_4^+$ ),  $(\text{benzene})_2$ , and  $\text{NH}_4^+–(\text{benzene})_2$  complexes in bulk water are performed using the polarizable models, in order to measure the strength of individual cation– $\pi$  and  $\pi–\pi$  interactions in water and to understand how one type of interaction affects the other.

## 2. METHODS

**2.1. Ab Initio Calculations.** The geometries of  $\text{Li}^+$ ,  $\text{Na}^+$ ,  $\text{K}^+$ , and  $\text{NH}_4^+$  in complex with water, benzene, and with the benzene dimer and trimer are optimized at the Møller–Plesset MP2/6-311++G(d,p) level with frozen core (FC) electrons, using Gaussian 09.<sup>43</sup> The interaction energies are corrected for basis set superposition error (BSSE) by the counterpoise method of Boys and Bernardi<sup>44</sup> (and referred to as  $E^{\text{CP}}$ ). Similar calculations are performed on the water–benzene complex and for the benzene dimer and trimer. The optimization of  $\text{Li}^+$ ,  $\text{Na}^+$ ,  $\text{K}^+$ , and  $\text{NH}_4^+$  in complex with benzene and with water is performed without imposing any geometry constraints. The optimization of the complexes with benzene dimer and trimer is performed imposing  $C_{6v}$  symmetry for the alkali metal ions and  $C_{2v}$  symmetry for the  $\text{NH}_4^+$  ion, such that the benzene molecules remain parallel and undisplaced. Optimization of benzene dimer and trimer is performed imposing  $D_{6h}$  symmetry as well. Although the cation– $(\text{benzene})_2$  and cation– $(\text{benzene})_3$  systems are not directly used to calibrate the polarizable models, they allow to further investigate the cooperativity between cation– $\pi$  and  $\pi–\pi$  interactions<sup>21,25</sup> and to test the performance of the polarizable force fields in describing such cooperativity. Two conformations of the cation– $(\text{benzene})_2$  systems are studied: the cation–benzene–benzene “stack” conformation and the benzene–cation–benzene “sandwich” conformation. The sandwich structures are optimized without any constraints, in both the straight and bent conformations.

Potential energy surfaces (PESs) of the four cation–benzene dimers and of the  $\text{NH}_4^+–\text{H}_2\text{O}$  dimer are calculated at the MP2(FC)/6-311++G(d,p) level, and all interaction energies are corrected for BSSE. The surfaces are computed with the molecular fragments kept in their optimized gas phase geometries, calculated at the same level of theory. PESs for the alkali metal cations are calculated by scanning both the perpendicular and parallel displacement of the ion relative to the benzene plane. For ammonium ion in complex with benzene, two potential curves are calculated. The first curve is calculated by scanning the distance between the nitrogen atom of  $\text{NH}_4^+$  (in its bidentate conformation) and the center of the benzene molecule (labeled X). The second curve is calculated by scanning the angle  $X \cdots N–H$ , which shows the interaction energy as a function of the orientation of the ion (unidentate, bidentate, or tridentate) on top of benzene surface. Two curves are calculated for the  $\text{NH}_4^+–\text{H}_2\text{O}$  complex by scanning the  $\text{N} \cdots \text{O}$  distance in the unidentate conformation of the ion and the orientation of  $\text{NH}_4^+$  relative

to O (unidentate, bidentate, or tridentate) at the optimal  $\text{N} \cdots \text{O}$  distance.

**2.2. Molecular Mechanical Calculations.** 2.2.1. *Potential Energy Function and Parametrization Strategy.* Molecular mechanics (MM) calculations are performed with the program CHARMM.<sup>45</sup> Polarizable models based on classical Drude oscillators<sup>40–42</sup> are parametrized for the interaction of the four cations ( $\text{Li}^+$ ,  $\text{Na}^+$ ,  $\text{K}^+$ , and  $\text{NH}_4^+$ ) with benzene and for the interaction of  $\text{NH}_4^+$  with water. For the interaction of  $\text{Li}^+$ ,  $\text{Na}^+$  and  $\text{K}^+$  with water, we use previously developed models.<sup>46</sup> Polarizability is introduced by attaching fictitious charged particles to all nonhydrogen atoms via a harmonic spring with force constant  $k_D$ . The partial charge of the polarizable atom,  $q$ , is distributed between the Drude particle and the atom core with the Drude particle charge  $q_D$  being determined from the atomic polarizability via the relation  $\alpha = q_D^2/k_D$ . The net charge of the atomic core is thus  $q_c = q - q_D$ . A separation  $d$  between the Drude particle and the polarizable atom results in an induced dipole moment  $q_Dd$ . The electrostatic energy term in the additive potential energy function<sup>47</sup> is modified to include interactions between atomic cores and Drude particles. A term describing the self-energy of a polarizable atom [ $1/2(k_Dd^2)$ ] is also added to the potential energy function.<sup>41</sup> The resulting potential energy function can be written as the following:<sup>47,48</sup>

$$U(R) = U_{\text{ion}}(R) + U_{\text{ion–solvent}}(R) + U_{\text{solvent}}(R) \quad (1)$$

where

$$\begin{aligned} U_{\text{ion}}(R) = & \frac{1}{2}k_D|\mathbf{r}_{\text{ion}} - \mathbf{r}_{D,\text{ion}}|^2 + \sum_{\text{NH bonds}} k_b(b - b_0)^2 \\ & + \sum_{\text{HNH angles}} k_\theta(\theta - \theta_0)^2 + \sum_{\text{HH pairs}} k_{\text{UB}}(s - s_0)^2 \end{aligned} \quad (2)$$

in which the last three terms are for  $\text{NH}_4^+$  only ( $b$  are NH bond lengths,  $\theta$  are HNH angles, and  $s$  are HH distances), and where

$$\begin{aligned} U_{\text{ion–solvent}}(R) = & \sum_{j=1}^N \sum_i \sum_s \left( \frac{q_{c,i}q_s}{|\mathbf{r}_i - \mathbf{r}_{js}|} + \frac{q_{D,j}q_s}{|\mathbf{r}_{D,j} - \mathbf{r}_{js}|} \right) \\ & + \sum_{j=1}^N \sum_i \sum_s E_{\min,js} \left[ \left( \frac{R_{\min,js}}{|\mathbf{r}_i - \mathbf{r}_{js}|} \right)^{12} - 2 \left( \frac{R_{\min,js}}{|\mathbf{r}_i - \mathbf{r}_{js}|} \right)^6 \right] \end{aligned} \quad (3)$$

in which  $N$  is the number of solvent molecules,  $i$  is the atomic site of the ion (Li, Na, K, N, H), and  $s$  is the solvent molecule site (atoms, lone pairs, Drude particles).  $U_{\text{solvent}}(R)$ , the third term in eq 1, is similarly obtained as the sum of bonded and nonbonded energy terms that correspond to interaction between atoms of the solvent molecules. Parameters in these equations and their definitions can be found in refs 47 and 48.

Parameters for the  $\text{NH}_4^+$  potential function are obtained based on ab initio calculations on the ion and its complex with benzene. The  $\text{NH}_4^+$  ion is modeled by five atomic sites and an auxiliary Drude particle attached to the nitrogen atom. Parameters  $b_0$ ,  $\theta_0$ , and  $s_0$  are set according to the ab initio geometry of the monomer in gas phase. NH bond stretching energy is represented by harmonic terms, and although these bonds are kept rigid during the simulations, the force constant  $k_b$  is adjusted to reproduce ab initio frequencies of the stretching modes. Angle bending terms are adjusted to reproduce the distortion energy associated with the bending modes. Urey–Bradley (UB) energy terms<sup>49</sup> are added to improve vibration frequencies and to prevent large

distortions in the tetrahedral structure of the ion. The electrostatic parameters (atomic charges and polarizabilities) are determined from ab initio calculation. The atomic charges are fitted to reproduce the traceless quadrupole moment of the ion, and the polarizability of N is calculated from the trace of the polarizability tensor.

Lennard-Jones (LJ) parameters of N and H atoms of ammonium are optimized separately for the interaction with benzene and water. Parameters of benzene are taken from ref 49. Parameters for the alkali metal ions are taken from ref 46. An extra nonatomic site (X) at the center of the benzene ring is required in order to accurately model the interactions with  $\text{Na}^+$  and  $\text{NH}_4^+$  ions. This site mimics the electron density at the center of the benzene ring and the repulsive effect it has on the ions. It is electrically neutral and shows a LJ interaction only with  $\text{Na}^+$  and with the N and H atoms of  $\text{NH}_4^+$ . The X site was not required for lithium, likely due to the small size of the ion and the close contact it forms with the benzene ring. It was also not required for potassium, which is too large to “discriminate” the steric profile of the ring.

The general parametrization strategy of the polarizable force field based on Drude oscillators has been documented elsewhere.<sup>41,42,46,49</sup> In the present work, the strength of the interaction of the four cations with benzene and of  $\text{NH}_4^+$  with water is adjusted by optimizing the LJ parameters between specific pairs of atoms of the monomers. The NBFIX<sup>45</sup> option of CHARMM allows assigning pair-specific LJ parameters  $E_{\min, is}$  and  $R_{\min, is}$  that override the default values obtained from the Lorentz–Berthelot combination rules:

$$E_{\min, is} = \sqrt{(E_{\min, i} E_{\min, s})} \quad \text{and} \quad R_{\min, is} = (R_{\min, i} + R_{\min, s})/2$$

Models for alkali metal–benzene interactions are optimized by adjusting pair-specific LJ parameters between the ions ( $\text{Li}^+$ ,  $\text{Na}^+$ , and  $\text{K}^+$ ) and the carbon atoms of benzene and between  $\text{Na}^+$  and the X site of benzene. Model for  $\text{NH}_4^+$ –benzene interaction is optimized by adjusting the LJ parameters of N and H atoms of  $\text{NH}_4^+$  as well as their pair-specific parameters with the X site in benzene. The interaction of  $\text{NH}_4^+$  with  $\text{H}_2\text{O}$  is optimized by adjusting pair-specific LJ parameters between N and H atoms of  $\text{NH}_4^+$  and oxygen atom of  $\text{H}_2\text{O}$ .

Parameter optimization uses the ab initio properties (complexation energies, geometries, and PESs) as targets and is performed in two steps. The first optimization step is to reproduce the ab initio PESs around their minimum. In this step the coordinates of the complex are kept rigid (at the values used for the ab initio potential energy scans), and the LJ parameters are adjusted to minimize the following error function:

$$\chi^2 = \sum_k (E_k^{\text{CP}} - E_k^{\text{MM}})^2 e^{-E_k^{\text{CP}}/k_B T}$$

where  $E_k^{\text{CP}}$  is the BSSE-corrected ab initio interaction energy,  $E_k^{\text{MM}}$  is the interaction energy from the polarizable model,  $k_B$  is Boltzmann constant, and  $T$  is the standard temperature (298.15 K). Index  $k$  represents the grid points on the potential energy surface. Minimization of this function leads to the best overall agreement between the interaction energies calculated from the Drude polarizable model ( $E_k^{\text{MM}}$ ) and the corresponding ab initio values ( $E_k^{\text{CP}}$ ). The sum of squared errors is weighted by a Boltzmann factor, which has the effect of increasing the importance of the low-energy conformations and ensures that the bottom of the energy surface is well reproduced.

The parameters obtained from this procedure are subjected to a second optimization step, in which the geometry and the

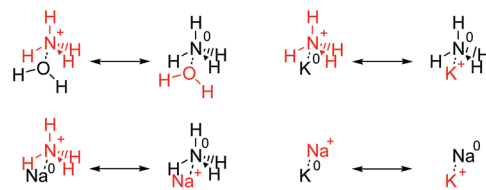


**Figure 1.** Solute transformations involved in the free energy calculations. Fragments in red are “real” while those in black are “dummy”. The dashed line represents the harmonic link.

interaction energy of the complex calculated without imposing geometry constraints (except fixing the bonds to H atoms using the SHAKE algorithm)<sup>50</sup> are fitted to the corresponding ab initio results. While the purpose of the first optimization step is to find the set of LJ parameters that gives the best global accuracy, the refined parameters resulting from the second step are more reliable, as they describe the geometry and the energetics of the complex under simulation conditions.

**2.2.2. MD Simulations.** MD simulations are performed in order to investigate cation– $\pi$ ,  $\pi$ – $\pi$ , and cation– $\pi_3$  interactions in water as well as the hydration structure of  $\text{NH}_4^+$ . All simulations are performed in the NPT ensemble at  $T = 298.15$  K and  $p = 1$  atm, with cubic periodic boundary conditions. Single ions are solvated in 250 water molecules; ion–benzene and benzene–benzene pairs and ion–benzene–benzene triples are solvated in 600 water molecules. The SWM4-NDP polarizable water model<sup>51</sup> is used for all simulations with a mass of 0.4 au on the auxiliary Drude particles and a force constant  $k_D = 1000$  kcal/mol/ $\text{\AA}^2$  for the atom–Drude coupling. Electrostatic interactions are computed using the particle-mesh Ewald method,<sup>52</sup> with  $\kappa = 0.34$  for the charge screening and a 1.0  $\text{\AA}$  grid spacing with fourth-order splines for the mesh interpolation. The real-space interactions (LJ and electrostatic) are cut off at 15  $\text{\AA}$ , and the long-range contribution from the LJ term is introduced as an average density-dependent term.<sup>53</sup> The temperature of the system is controlled with a two-thermostat algorithm, where atoms are kept at room temperature (298.15 K) and auxiliary Drude particles are kept at low temperature (1 K) to ensure self-consistent dipole induction.<sup>41</sup> The equations of motion are integrated using a 1 fs time step, with all bonds involving hydrogen atoms kept at their reference lengths using the SHAKE algorithm.<sup>50</sup>

**2.2.3. Free Energy Calculations.** The polarizable model for the  $\text{NH}_4^+$ – $\text{H}_2\text{O}$  complex is validated by calculating the free energy of hydration of an  $\text{NH}_4^+$  ion relative to  $\text{H}_2\text{O}$ ,  $\text{Na}^+$ , and  $\text{K}^+$ . Free energy calculations are performed following the thermodynamic integration (TI) simulation protocol established previously.<sup>48</sup> In particular, the relative hydration free energy ( $\Delta\Delta G_{\text{hydr}}$ ) of solutes A and B is evaluated from the conventional thermodynamic cycle for solute transformation in water:

$$\Delta\Delta G_{\text{hydr}}(\text{A} \rightarrow \text{B}) \equiv \Delta G_{\text{hydr}}(\text{B}) - \Delta G_{\text{hydr}}(\text{A}) = \Delta G_{\text{mut}}^{\text{wat}}$$

where  $\Delta G_{\text{mut}}^{\text{wat}}$  is the relative free energy for the alchemical  $\text{A} \rightarrow \text{B}$  “mutation” in water.

To maintain a constant number of interaction sites throughout the transformation, special hybrid residues are used (see Figure 1) in which A and B solutes are linked through their heavy atoms via a weak harmonic bond of force constant 5 kcal/mol/ $\text{\AA}^2$ . These residues are formed by tethering one original “real” ion with a “dummy” ion having no interactions with the real particles. The mutation simply involves “turning off” the nonbonded

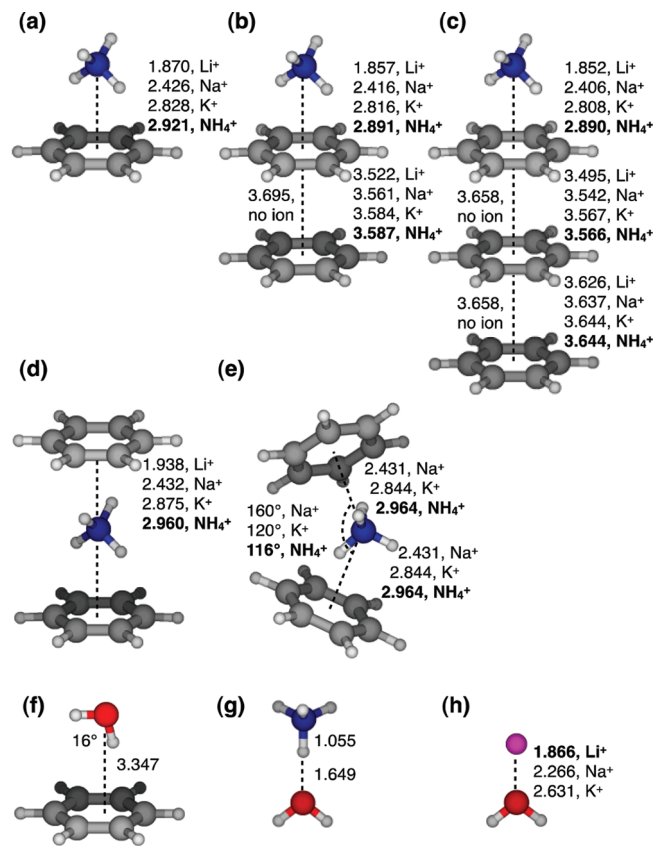


**Figure 2.** Optimized geometries at MP2(FC)/6-311++G(d,p) level of theory for the (a) cation–benzene, (b) cation–(benzene)<sub>2</sub>, (c) cation–(benzene)<sub>3</sub>, (d) benzene–cation–benzene, (e) benzene–cation–benzene bent sandwich (unstable for Li<sup>+</sup>), (f) water–benzene, (g) ammonium–water, and (h) alkali ion–water complexes. The structures of panels (a–e) are illustrated with NH<sub>4</sub><sup>+</sup> complexes, but corresponding parameters for the lithium, sodium, and potassium complexes are reported.

parameters of the real fragment while “turning on” those of the dummy fragment. The ligand transformation is performed in 17 steps, controlled by a scaling parameter  $\lambda$  which takes the following values: 0, 0.002, 0.005, 0.05, 0.1, 0.2, 0.3, 0.4, 0.5, 0.6, 0.7, 0.8, 0.9, 0.95, 0.995, 0.998, and 1. Each  $\lambda$  window is equilibrated for 150 ps followed by subsequent data collection for 350 ps.

**2.2.4. Potential of Mean Force Calculations.** Potentials of mean force (PMFs) between each cation (Li<sup>+</sup>, Na<sup>+</sup>, K<sup>+</sup>, or NH<sub>4</sub><sup>+</sup>) and one benzene molecule and between two benzene molecules are calculated using umbrella sampling. The distance between the centers of mass (CMs) of the reactants is used as a reaction coordinate, and a harmonic potential of force constant 10 kcal/mol/Å<sup>2</sup> is applied to bias the sampling. The reaction coordinate is sampled using 0.5 Å separated windows, and each window is simulated for 2 ns. The unbiased PMF is reconstructed using the weighted histogram analysis method (WHAM),<sup>54,55</sup> and the radial variation in the entropy of the solute pairs is taken into account by adding a  $2k_B T \ln(R)$  correction term to the PMF.<sup>56</sup>

### 3. RESULTS AND DISCUSSION

**3.1. Ab Initio Interaction Energies.** The optimized geometries of all studied complexes and some of their structural parameters are presented in Figure 2. BSSE-corrected and -uncorrected complexation energies ( $E^{\text{CP}}$  and  $E$ , respectively) and equilibrium

**Table 1.** Ab Initio Complexation Energies and Equilibrium Distances ( $R_1$ ,  $R_2$ ,  $R_3$ ) Calculated at the MP2(FC)/6-311++G(d,p) Level of theory and Corresponding Energies Calculated Using the Polarizable Models ( $E^{\text{MM}}$ )<sup>a</sup>

complex	$E$	$E^{\text{CP}}$	$R_1$	$R_2$	$R_3$	$E^{\text{MM}}$
benz–Li <sup>+</sup>	−38.84	−34.89	1.870	—	—	−35.14
benz–Na <sup>+</sup>	−24.00	−21.08	2.426	—	—	−21.04
benz–K <sup>+</sup>	−19.58	−17.14	2.828	—	—	−17.01
benz–NH <sub>4</sub> <sup>+</sup>	−19.78	−17.58	2.921	—	—	−17.56
(benz) <sub>2</sub> –Li <sup>+</sup>	−49.00	−41.48	1.857	3.522	—	−40.59
(benz) <sub>2</sub> –Na <sup>+</sup>	−32.92	−26.65	2.416	3.561	—	−25.66
(benz) <sub>2</sub> –K <sup>+</sup>	−28.31	−22.23	2.816	3.584	—	−21.25
(benz) <sub>2</sub> –NH <sub>4</sub> <sup>+</sup>	−28.67	−22.82	2.891	3.587	—	−21.84
benz–Li <sup>+</sup> –benz	−71.88	−60.57	1.938	—	—	−62.47
benz–Na <sup>+</sup> –benz	−46.50	−38.86	2.432	—	—	−40.16
benz–K <sup>+</sup> –benz	−37.56	−32.09	2.875	—	—	−33.09
benz–NH <sub>4</sub> <sup>+</sup> –benz	−37.33	−32.17	2.960	—	—	−32.70
(benz) <sub>3</sub> –Li <sup>+</sup>	−56.12	−44.72	1.852	3.495	3.626	−43.62
(benz) <sub>3</sub> –Na <sup>+</sup>	−39.73	−29.63	2.406	3.542	3.637	−28.50
(benz) <sub>3</sub> –K <sup>+</sup>	−34.98	−25.10	2.808	3.567	3.644	−24.00
(benz) <sub>3</sub> –NH <sub>4</sub> <sup>+</sup>	−35.37	−25.69	2.890	3.566	3.644	−24.63
(benz) <sub>2</sub>	−4.94	−1.79	—	3.695	—	−2.07
(benz) <sub>3</sub>	−10.67	−3.62	—	3.658	3.658	−4.20
benz–H <sub>2</sub> O	−4.52	−2.43	3.347	—	—	−2.68 <sup>b</sup>
H <sub>2</sub> O–Li <sup>+</sup>	−35.50	−33.40	1.866	—	—	−35.92 <sup>b</sup>
H <sub>2</sub> O–Na <sup>+</sup>	−24.67	−23.09	2.266	—	—	−24.64 <sup>b</sup>
H <sub>2</sub> O–K <sup>+</sup>	−18.93	−17.88	2.631	—	—	−17.90 <sup>b</sup>
H <sub>2</sub> O–NH <sub>4</sub> <sup>+</sup>	−22.16	−20.27	2.704	—	—	−20.28

<sup>a</sup>  $E$ : uncorrected; and  $E^{\text{CP}}$ : BSSE-corrected. All energies in kcal/mol and all distances in Å. <sup>b</sup> Calculated using the original polarizable models.<sup>46,49,51</sup> <sup>c</sup> Bent sandwich geometry of the complex (see Figure 2e). The Li<sup>+</sup> complex is unstable.

distances ( $R_1$ ,  $R_2$ , and  $R_3$ ) are reported in Table 1. The complexation energies and equilibrium distances for the (benzene)<sub>2</sub>, (benzene)<sub>3</sub>, and benzene–H<sub>2</sub>O complexes are also reported in Table 1. The three equilibrium distances,  $R_1$ ,  $R_2$ , and  $R_3$ , represent CM separations between the cation and the closest benzene molecule, between the closest and second closest benzene molecules, and between the second and third closest benzene molecules, respectively.  $R_1$  is also assigned to the CM separation between the cations and water and between water and benzene. As reported in Table 1, the MP2(FC)/6-311++G(d,p) interaction energies of Li<sup>+</sup>, Na<sup>+</sup>, K<sup>+</sup>, and NH<sub>4</sub><sup>+</sup> with benzene monomer are −34.89, −21.08, −17.14, and −17.58 kcal/mol, respectively. Although these values are simple interaction energies (neglecting thermodynamic contributions), they are comparable to the corresponding experimental gas phase binding enthalpies (at 298 K) of  $-39.3 \pm 3.2$ ,  $-22.5 \pm 1.5$ ,  $-17.7 \pm 1.0$ , and  $-19.3 \pm 1.0$  kcal/mol.<sup>7,10</sup>

For alkali cation complexes, the interaction energy decreases (that is, becomes less negative) while  $R_1$  increases on going from Li<sup>+</sup> to K<sup>+</sup> (see Table 1), which can be attributed to the increase of the cation size. For a given cation, the interaction energy increases on going from benzene monomer to trimer complexes, while  $R_1$ ,  $R_2$ , and  $R_3$  decrease (see Table 1 and Figure 2a, b, and c).

**Table 2.** BSSE-Corrected Complexation Energies Calculated at the MP2(FC)/6-311++G(d,p) Level and Corresponding Interaction Energies Calculated Using the Polarizable Models (in parentheses)<sup>a</sup>

complex	$E_{\text{tot}}$	$E_{\text{M}-\text{B}_1}$	$E_{\text{M}-\text{B}_2}$	$E_{\text{M}-\text{B}_3}$	$E_{\text{B}_1-\text{B}_2}$	$E_{\text{B}_2-\text{B}_3}$	$E_{\text{B}_1-\text{B}_3}$	$E_{\text{coop}}$
benz-Li <sup>+</sup>	-34.89 (-35.14)	-34.89 (-35.14)	—	—	—	—	—	—
benz-Na <sup>+</sup>	-21.08 (-21.04)	-21.08 (-21.04)	—	—	—	—	—	—
benz-K <sup>+</sup>	-17.14 (-17.01)	-17.14 (-17.01)	—	—	—	—	—	—
benz-NH <sub>4</sub> <sup>+</sup>	-17.58 (-17.56)	-17.58 (-17.56)	—	—	—	—	—	—
(benz) <sub>2</sub> -Li <sup>+</sup>	-41.48 (-40.59)	-34.82 (-34.93)	-4.26 (-2.90)	—	-1.10 (-0.63)	—	—	-1.30 (-2.13)
(benz) <sub>2</sub> -Na <sup>+</sup>	-26.65 (-25.66)	-21.02 (-20.97)	-3.12 (-2.15)	—	-1.35 (-1.00)	—	—	-1.16 (-1.54)
(benz) <sub>2</sub> -K <sup>+</sup>	-22.23 (-21.25)	-17.09 (-17.02)	-2.59 (-1.84)	—	-1.47 (-1.18)	—	—	-1.08 (-1.21)
(benz) <sub>2</sub> -NH <sub>4</sub> <sup>+</sup>	-22.82 (-21.84)	-17.56 (-18.24)	-2.57 (-1.81)	—	-1.48 (-1.20)	—	—	-1.21 (-0.59)
benz-Li <sup>+</sup> -benz	-60.57 (-62.47)	-34.79 (-34.66)	-34.79 (-34.66)	—	-1.90 (-2.05)	—	—	10.91 (8.90)
benz-Na <sup>+</sup> -benz	-38.86 (-40.16)	-20.99 (-20.98)	-20.99 (-20.98)	—	-0.75 (-1.04)	—	—	3.87 (2.82)
	-38.85 <sup>b</sup>	-20.99 <sup>b</sup>	-20.99 <sup>b</sup>	—	-0.89 <sup>b</sup>	—	—	4.02 <sup>b</sup>
	(-39.04) <sup>b</sup>	(-20.61) <sup>b</sup>	(-20.61) <sup>b</sup>	—	(-1.19) <sup>b</sup>	—	—	(3.37) <sup>b</sup>
benz-K <sup>+</sup> -benz	-32.09 (-33.09)	-17.17 (-17.12)	-17.17 (-17.12)	—	-0.20 (-0.44)	—	—	2.45 (1.59)
	-32.26 <sup>b</sup>	-17.15 <sup>b</sup>	-17.15 <sup>b</sup>	—	-0.83 <sup>b</sup>	—	—	2.87 <sup>b</sup>
	(-33.07) <sup>b</sup>	(-17.10) <sup>b</sup>	(-17.10) <sup>b</sup>	—	(-1.14) <sup>b</sup>	—	—	(2.27) <sup>b</sup>
benz-NH <sub>4</sub> <sup>+</sup> -benz	-32.17 (-32.07)	-17.39 (-17.37)	-17.42 (-17.35)	—	-0.13 (-0.35)	—	—	2.77 (3.00)
	-31.80 <sup>b</sup>	-16.99 <sup>b</sup>	-16.99 <sup>b</sup>	—	-0.78 <sup>b</sup>	—	—	2.96 <sup>b</sup>
	(-31.59) <sup>b</sup>	(-16.23) <sup>b</sup>	(-16.23) <sup>b</sup>	—	(-1.14) <sup>b</sup>	—	—	(2.01) <sup>b</sup>
(benz) <sub>3</sub> -Li <sup>+</sup>	-44.72 (-43.62)	-34.80 (-34.92)	-4.35 (-2.97)	-0.93 (-0.60)	-0.93 (-0.36)	-1.63 (-1.45)	-0.001 (-0.12)	-2.08 (-3.20)
(benz) <sub>3</sub> -Na <sup>+</sup>	-29.63 (-28.50)	-20.99 (-20.91)	-3.18 (-2.20)	-0.76 (-0.49)	-1.26 (-0.85)	-1.66 (-1.50)	-0.002 (-0.12)	-1.78 (-2.43)
(benz) <sub>3</sub> -K <sup>+</sup>	-25.10 (-24.00)	-17.09 (-17.00)	-2.64 (-1.87)	-0.66 (-0.44)	-1.39 (-1.06)	-1.68 (-1.53)	-0.003 (-0.11)	-1.64 (-1.99)
(benz) <sub>3</sub> -NH <sub>4</sub> <sup>+</sup>	-25.69 (-24.63)	-17.55 (-18.23)	-2.60 (-1.84)	-0.65 (-0.43)	-1.39 (-1.05)	-1.68 (-1.54)	-0.003 (-0.12)	-1.82 (-1.42)

<sup>a</sup>  $E_{\text{tot}}$  is the total complexation energy,  $E_{\text{A-B}}$  are complexation energies of the different fragment pairs, and  $E_{\text{coop}}$  is the cooperativity [see eq 4]. All energies in kcal/mol. <sup>b</sup> Bent sandwich geometry of the complex (see Figure 2e). The Li<sup>+</sup> complex is unstable.

The values of  $R_1$  reported in Table 1 for Li<sup>+</sup>, Na<sup>+</sup>, and K<sup>+</sup> complexes with benzene (1.870, 2.426, and 2.828 Å, respectively) are in close agreement with the distances calculated by Feller et al.<sup>17</sup> at the MP2/CBS level of theory (1.879, 2.390, and 2.786 Å, respectively).

Table 1 shows that cations are always closer to the benzene molecule ( $R_1$  shorter) in cation-dimer complexes than in cation-monomer complexes and that two benzene molecules are always closer ( $R_2$  shorter) in cation-dimer complexes than in the benzene-dimer. This indicates that cation-π and π-π interactions stabilize one another and that cooperativity between the two interactions contributes to the overall stabilization of the system.<sup>21</sup>

By comparison, the sandwich benzene-cation-benzene complexes (see Figure 2d and e), while more stable than

the cation-benzene-benzene conformers, display competitive cation-π interactions. For instance, the straight sandwich ammonium complex has a total complexation energy less than twice that of the NH<sub>4</sub><sup>+</sup>-benzene pair (-32.17 kcal/mol, compared to  $2 \times -17.58 = -35.16$  kcal/mol), and the cation-benzene distances are larger (2.960 Å, compared to 2.921 Å for the NH<sub>4</sub><sup>+</sup>-benzene pair). The bent sandwich conformation, almost iso-energetic to the straight conformation, displays similar competitiveness. It is important for a molecular model to reproduce these effects, as the cooperation between cation-π and π-π interactions and the competition between two cation-π interactions are not expected to play out the same way in aqueous solution as in gas phase.

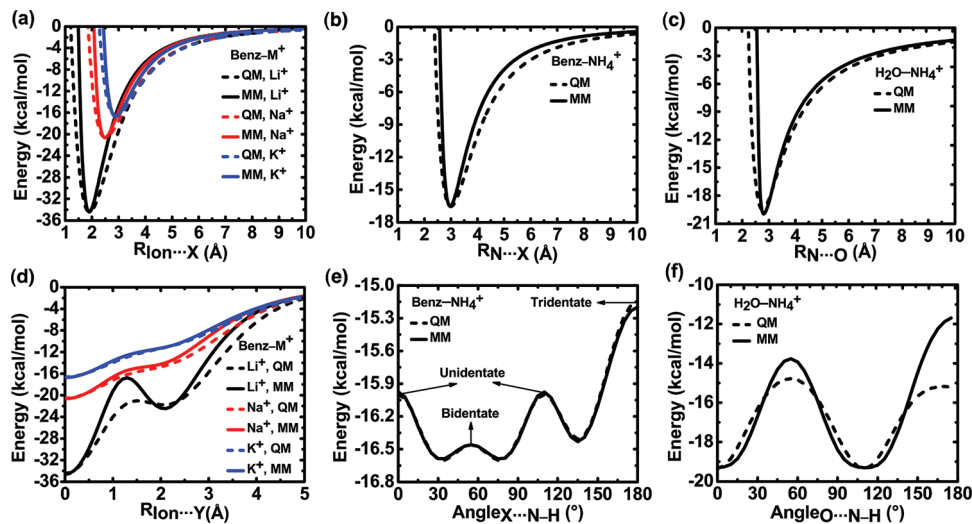


**Figure 3.** Potential energy curves for benzene–M<sup>+</sup> (M<sup>+</sup> = Li<sup>+</sup>, Na<sup>+</sup>, K<sup>+</sup>, or NH<sub>4</sub><sup>+</sup>) and H<sub>2</sub>O–NH<sub>4</sub><sup>+</sup> complexes from ab initio MP2(FC)/6-311++G(d,p) calculations (dashed line) and from polarizable model (solid line). The following coordinates are scanned: (a) in benzene–M<sup>+</sup> complex, X···M<sup>+</sup> distance in the direction perpendicular to the benzene plane (X is the center of the benzene ring); (b) in benzene–NH<sub>4</sub><sup>+</sup> complex, X···N distance between the benzene center and the nitrogen atom of NH<sub>4</sub><sup>+</sup> in its bidentate conformation; (c) in H<sub>2</sub>O–NH<sub>4</sub><sup>+</sup> complex, O···N distance; (d) in benzene–M<sup>+</sup> complex, Y···M<sup>+</sup> distance in the direction parallel to the benzene plane (Y is the equilibrium position of the ion; see Figure 2a), going toward the C–C bond center; (e) in benzene–NH<sub>4</sub><sup>+</sup> complex, X···N–H angle for NH<sub>4</sub><sup>+</sup> on top of benzene at X···N distance = 3.0 Å; and (f) in H<sub>2</sub>O–NH<sub>4</sub><sup>+</sup> complex, O···N–H angle at O···N distance = 2.7 Å.

We evaluate  $E_{\text{coop}}$ , the cooperation energy of a complex, as the difference between  $E_{\text{tot}}$ , the total complexation energy, and the sum of all pairwise interaction energies in the complex:

$$E_{\text{coop}} = E_{\text{tot}} - \left( \sum_m E_{\text{M-B}_m} + \sum_{m < m'} E_{\text{B}_m-\text{B}_{m'}} \right) \quad (4)$$

where  $m$  and  $m'$  label the benzene molecules (see Table 2).  $E_{\text{M-B}_m}$  is the complexation energy of the different ion–benzene pairs and  $E_{\text{B}_m-\text{B}_{m'}}$  is the complexation energy of the different benzene pairs—whether they are in contact or not. These energies are calculated at the geometry obtained from the optimization of the whole complex and corrected for BSSE.

Table 2 shows that the sign and the magnitude of  $E_{\text{coop}}$  depends on the nature of the complex. Parallel stacked cation–(benzene)<sub>2</sub> and cation–(benzene)<sub>3</sub> complexes show negative  $E_{\text{coop}}$ , which indicates that the two interactions strengthens one another.<sup>25</sup> The positive  $E_{\text{coop}}$  observed in the sandwich complexes of the benzene dimer indicates on the other hand that the two interactions are competitive.

This cooperative or anticooperative behavior is related to the polarization of the benzene molecules. Table 2 also reports the interaction energies calculated using the optimized Drude models (see Section 3.3). In the stacked conformation of the NH<sub>4</sub><sup>+</sup>–(benzene)<sub>2</sub> complex, the polarizable model induces a dipole of +2.53 D in the first benzene ring and of +0.60 D in the second. Those two dipoles are parallel and result in a stabilization of the complex by 0.59 kcal/mol (compared to 1.21 kcal/mol from the ab initio calculations). In the straight sandwich conformation, the ion induces antiparallel dipoles of +2.01 and –2.01 D, which destabilizes the complex by 3.00 kcal/mol (compared to 2.77 kcal/mol from the ab initio calculations). This behavior cannot be reproduced with a conventional, nonpolarizable force field.

**3.2. Ab Initio Potential Energy Surfaces.** Ab initio potential energy curves for Li<sup>+</sup>, Na<sup>+</sup>, K<sup>+</sup>, and NH<sub>4</sub><sup>+</sup> in complex with benzene monomer and for NH<sub>4</sub><sup>+</sup> in complex with H<sub>2</sub>O are reported in Figure 3, along with the corresponding curves

obtained from the optimized Drude models (see Section 3.3). Two curves are calculated for the interactions of the alkali cations with the benzene monomer (Figure 3a and d). Curve 3a is calculated by positioning the cation on top of the benzene center, along the six-fold symmetry axis, and by scanning the distance  $R$  between the cation and the ring centroid (site X) from 1.0 to 10.0 Å. This curve indicates that the depth and the extent of the potential energy well depends on the size of the cation and on its ability to approach the electron cloud of benzene.<sup>20</sup> Curve 3d is calculated by positioning the alkali cations on top of the benzene center at the equilibrium separation distances (called site Y) and scanning the movement of the cations parallel to the benzene ring, going toward the C–C bond center. This curve confirms that, although the interaction energy decreases as the cation moves away from the benzene center, the complex remains stable.<sup>24</sup>

Two potential curves are calculated for ammonium–benzene complex (Figure 3b and e). Curve 3b is calculated by scanning the X···N distance with ammonium in the bidentate orientation. Curve 3e is generated by scanning the X···N–H angle and describes the interaction energy of the complex as a function of ammonium orientation: unideterminate (0° and 109°), bidentate (55°), and trideterminate (180°). This curve shows that the stability of the different ammonium conformers follows the order bidentate > unideterminate > trideterminate. The global minimum conformer however displays an angle X···N–H of 35° or 75°, corresponding to an ammonium orientation between the exact unideterminate and bidentate conformations.

Two potential curves are calculated for the NH<sub>4</sub><sup>+</sup>–H<sub>2</sub>O complex (Figure 3c and f). Curve 3c shows the scan of the N···O distance in the ammonium unideterminate orientation, from 2.0 to 10.0 Å. Curve 3f shows the scan of angle O···N–H from 0° to 180°, so as to investigate the relative stability of the unideterminate (0° and 109°), bidentate (55°), and trideterminate (180°) conformers. According to the QM calculations, the

**Table 3.** Pair-Specific LJ Parameters for the Interactions of  $\text{Li}^+$ ,  $\text{Na}^+$ ,  $\text{K}^+$ , and  $\text{NH}_4^+$  with Benzene and Water<sup>a</sup>

ion	i	$E_{\min}$ (kcal/mol)	$R_{\min}/2$ (Å)	ion–benzene interaction				ion–water interaction	
				$E_{\min,iC}$ (kcal/mol)	$R_{\min,iC}$ (Å)	$E_{\min,iX}$ (kcal/mol)	$R_{\min,iX}$ (Å)	$E_{\min,iO}$ (kcal/mol)	$R_{\min,iO}$ (Å)
$\text{NH}_4^+$	N	2.387030	1.306271	0.4058387 <sup>b</sup>	3.3962713 <sup>b</sup>	0.1470587	3.5005950	0.1018465	3.7592014
	H	0.003998	1.087051	0.0109515 <sup>b</sup>	2.3562713 <sup>b</sup>	0.0060183	3.2808392	0.0092367	2.8848120
$\text{Li}^+$	Li	0.030000	1.100000	0.0644005	3.1950579	0.0	0.0	0.0795506 <sup>c</sup>	2.8869290 <sup>c</sup>
$\text{Na}^+$	Na	0.0315100	1.461680	0.2004369	3.3592376	0.0099919	3.6398984	0.0815280 <sup>c</sup>	3.2486090 <sup>c</sup>
$\text{K}^+$	K	0.1419265	1.686652	0.4266716	3.5744944	0.0	0.0	0.1730273 <sup>c</sup>	3.4735811 <sup>c</sup>

<sup>a</sup> Parameters with hydrogen atoms of benzene and water are obtained using the Lorentz–Berthelot mixing rules. <sup>b</sup> Obtained from benzene parameters<sup>49</sup> using the Lorentz–Berthelot mixing rules. <sup>c</sup> Obtained from alkali cations<sup>48</sup> and water<sup>51</sup> parameters using the Lorentz–Berthelot mixing rules.

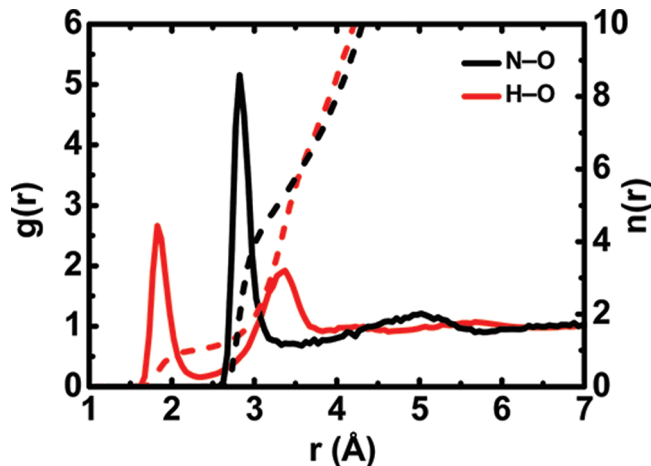


**Figure 4.** N–O and H–O radial distribution functions (solid lines, scale on left) and running integration numbers (dashed lines, scale on right) of  $\text{NH}_4^+$  in water at 298.15 K.

stability of the conformers follows the order unidentate > bidentate  $\sim$  tridentate.

**3.3. Optimized Force Field.** Equilibrium structural parameters for the potential model of  $\text{NH}_4^+$  (see eq 2) are obtained from ab initio optimization of the ion in the gas phase at the MP2/6-311+G(d,p) level of theory:  $b_0 = 1.024 \text{ \AA}$ ,  $\theta_0 = 109.47^\circ$ , and  $s_0 = 1.673 \text{ \AA}$ . Bond, angle, and UB force constants are fitted in CHARMM<sup>45</sup> based on ab initio calculated IR frequencies of gaseous  $\text{NH}_4^+$  ( $\nu = 3 \times 1496, 2 \times 1734, 3413$ , and  $3 \times 3547 \text{ cm}^{-1}$ ). Parameters  $k_b = 470 \text{ kcal/mol/\AA}^2$ ,  $k_\theta = 25 \text{ kcal/mol/rad}^2$ , and  $k_{UB} = 9 \text{ kcal/mol/\AA}^2$  are chosen because they yield comparable IR frequencies ( $\nu = 3 \times 1716, 2 \times 1940, 3461$ , and  $3 \times 3546 \text{ cm}^{-1}$ ) and maintain structural stability of the ion during MD simulations. Although these frequencies are overestimating the ab initio bending vibrational frequencies of the ion ( $1496$  and  $1734 \text{ cm}^{-1}$ ), they reproduce the ab initio angle bending energies with less than 20% error. Since ab initio calculations of the hydration of ammonium in water clusters show that the HNH angles do not systematically bend by more than a fraction of a degree,<sup>57</sup> this represents an error of less than 0.01 kcal/mol.

Nonbonded parameters (atomic charges, polarizability, and LJ parameters) of the polarizable ammonium model are determined based on ab initio calculations on the gaseous ion and its complex with benzene and found to be  $q(\text{H}) = 0.64413 \text{ e}$ ,  $q(\text{N}) = -1.57652 \text{ e}$ ,  $\alpha_{\text{N}} = 1.1966 \text{ \AA}^3$ ,  $E_{\min}(\text{N}) = 2.387030 \text{ kcal/mol}$ ,  $R_{\min}(\text{N})/2 = 1.306271 \text{ \AA}$ ,  $E_{\min}(\text{H}) = 0.003998 \text{ kcal/mol}$ , and  $R_{\min}(\text{H})/2 = 1.087051 \text{ \AA}$ .

**Table 4.** Relative Hydration Free Energies (in kcal/mol) As Calculated from TI/MD Simulations in Bulk Water and Corresponding Experimental Values

mutation	$\Delta G_{\text{mut}}^{\text{wat}}$	experiment
$\text{NH}_4^+ \rightarrow \text{H}_2\text{O}$	61.7	$61.8^{62a}, 65.6^{60a}$
$\text{NH}_4^+ \rightarrow \text{Na}^+$	-18.6	$-18.1^{59}, -19.1^{62}$
$\text{NH}_4^+ \rightarrow \text{K}^+$	-1.2	$-0.5^{59}, -2.4^{62}$
$\text{Na}^+ \rightarrow \text{K}^+$	16.7	$16.7^{62}, 17.2^{63}, 17.6^{59,61}$

<sup>a</sup> Calculated using  $-6.32 \text{ kcal/mol}$  as the experimental hydration free energy of water.<sup>64</sup>

Optimized pair-specific LJ parameters for the interaction of the four cations ( $\text{Li}^+$ ,  $\text{Na}^+$ ,  $\text{K}^+$ , and  $\text{NH}_4^+$ ) with benzene and for  $\text{NH}_4^+–\text{H}_2\text{O}$  interaction are listed in Table 3. These parameters are first optimized based on the ab initio PESs and then refined to reproduce the ab initio geometry and interaction energy in the global minimum complex (see columns “ $E^{\text{CP}}$ ” and “ $E^{\text{MM}}$ ” of Table 1). The models also reproduce the ab initio PESs, as shown in Figure 3. Because of the intrinsic limitations of LJ potentials at reproducing both the position of the energy minimum and its curvature, the molecular models that yield correct binding energy, and equilibrium distance are systematically underestimating long-range interactions (see Figure 3a and b). For this reason, the interaction of the four cations with the benzene dimer in the stacked conformation (for which the second benzene molecule is about 6 Å away from the ion) is underestimated by about 1 kcal/mol. However, this systematic error does not increase with the stacking of a third benzene molecule, as the deviation between  $E^{\text{MM}}$  and  $E^{\text{CP}}$  becomes negligible at larger distances (see Figure 3a and b).

**3.4. Hydration of  $\text{NH}_4^+$ .** The optimized model for  $\text{NH}_4^+–\text{H}_2\text{O}$  interaction reproduces the ab initio calculated complexation energy and PESs (see Table 1 and Figure 3c and f). To further validate the model, the solvation structure of the ion in water and its free energy of hydration relative to  $\text{H}_2\text{O}$ ,  $\text{Na}^+$ , and  $\text{K}^+$  are calculated.

The solvation structure of the ammonium ion is investigated from the analysis of the last 7 ns of a 10 ns MD simulation of one ion solvated in 250 SWM4-NDP water molecules. The pair correlation functions  $g_{\text{NO}}(r)$  and  $g_{\text{HO}}(r)$  (where N and H refer to  $\text{NH}_4^+$ ) are reported in Figure 4. Function  $g_{\text{NO}}(r)$  shows a maximum at 2.85 Å and a minimum at 3.37 Å. Integration up to this minimum yields a coordination number of 5.3, in excellent agreement with ab initio MD studies,<sup>58</sup> which report a coordination number of 5.3 as well. Function  $g_{\text{HO}}(r)$  shows a first peak at 1.85 Å and a minimum at 2.36 Å. Integration yields a coordination number of 1.05, corresponding to one water molecule

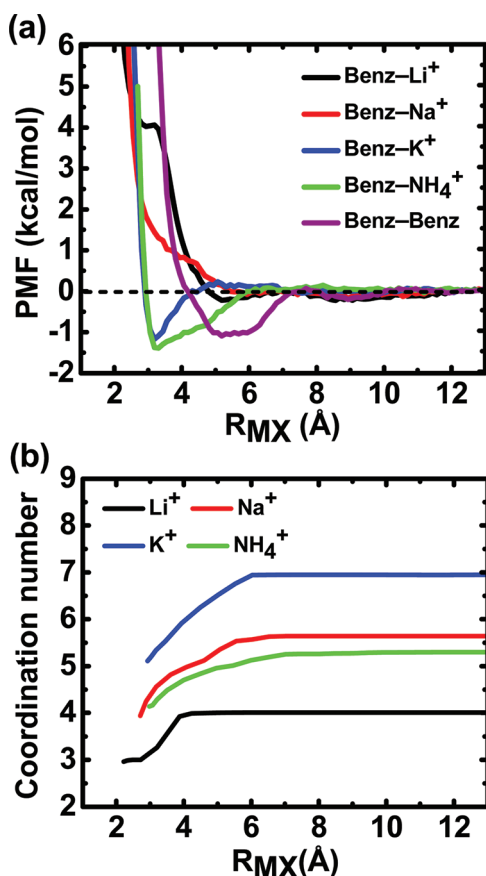


**Figure 5.** (a) PMFs between the centers of ions and benzene and between the centers of two benzene molecules in water. (b) Water-coordination number of  $\text{Li}^+$ ,  $\text{Na}^+$ ,  $\text{K}^+$ , and  $\text{NH}_4^+$  ions as a function of their center-of-mass separation from a benzene molecule.

hydrogen-bonded to every proton of  $\text{NH}_4^+$ , forming a tetrahedral structure around the ion. This suggests that the additional 1.3 water molecules found inside the N–O coordination sphere are much more mobile, in agreement with previous results from ab initio MD simulations.<sup>58</sup>

Reliable simulations of ions in aqueous solution require models that reproduce their free energy of hydration ( $\Delta G_{\text{hydr}}$ ). To further validate the  $\text{NH}_4^+–\text{H}_2\text{O}$  potential model, we calculate the change in free energy of hydration associated with mutation of  $\text{NH}_4^+$  to  $\text{H}_2\text{O}$ ,  $\text{Na}^+$ , or  $\text{K}^+$ . As a control for the “hybrid residue” method used (see Section 2.2.3), the change in free energy for mutating  $\text{Na}^+$  to  $\text{K}^+$  is also calculated and compared to published values obtained using a different protocol.<sup>46</sup> The results are reported in Table 4, along with corresponding experimental and computational data.<sup>59–64</sup> On the basis of multiple runs (forward and backward), the error on the calculated values is of the order of 0.1 kcal/mol.

The data in Table 4 show good agreement between the calculated and experimental data. Taking into account the hydration free energy of the SWM4-NDP water molecule,  $-5.9 \pm 0.1$  kcal/mol,<sup>51</sup> this results in a hydration free energy of  $\text{NH}_4^+$  equal to  $-67.6$  kcal/mol, in agreement with the experimental value of  $-68.1$  kcal/mol reported by Marcus.<sup>62</sup> It should be noted that the  $\text{NH}_4^+–\text{H}_2\text{O}$  interaction model was not optimized to reproduce these experimental results; parametrization was aimed at reproducing the ab initio properties of the  $\text{NH}_4^+–\text{H}_2\text{O}$  complex only. This further confirms the transferability of the parametrized  $\text{NH}_4^+–\text{H}_2\text{O}$  model

from gas phase to aqueous phase. More importantly, the model reproduces the hydration free energy relative to  $\text{Na}^+$  and  $\text{K}^+$  (see Table 4), which ensures that the affinities for both water and benzene are correctly represented across the ion series.

**3.5. Cation– $\pi$  Interactions in Aqueous Solution.** Compared to the gas phase interaction energies reported in Table 1, cation– $\pi$  interactions are much weaker in aqueous solution,<sup>19,37–39</sup> due to competing interactions with water. In the gas phase, the interaction energies of the alkali cations with benzene follow the order  $\text{Li}^+ > \text{Na}^+ > \text{K}^+$  (see Table 1). In water, the cation– $\pi$  affinity is reported<sup>1,65</sup> to show the reverse order:  $\text{K}^+ \gg \text{Na}^+ \sim \text{Li}^+$ .

The binding affinity of the four studied cations with benzene in water is estimated from PMF calculations (see Figure 5a). Our finding for the binding free energies of  $\text{Li}^+$ ,  $\text{Na}^+$ , and  $\text{K}^+$  with benzene in water is in agreement with the expected trend.<sup>65</sup>  $\text{Li}^+$  and  $\text{Na}^+$  do not associate with benzene in presence of water, as evidenced by the absence of a free energy minimum near the gas phase calculated equilibrium distances. For  $\text{Li}^+$ , the shallow minimum ( $-0.2$  kcal/mol) observed at CM separation of  $5.1$  Å can be interpreted as a weak interaction of benzene with the “dressed”, tetraqua  $\text{Li}^+$  ion. At that distance, the interaction energy of  $\text{Li}^+$  with benzene, as calculated from the PES, is  $-4.7$  kcal/mol (see Figure 3a). Benzene in the second solvation shell of the ion will thus be stabilized by the interaction with ion-coordinated water molecules in addition to the long-distance interaction with the cation.  $\text{K}^+$  and  $\text{NH}_4^+$ , on the other hand, bind benzene in water with energies of  $-1.2$  and  $-1.4$  kcal/mol at equilibrium CM separations of  $3.2$  and  $3.3$  Å, respectively. These equilibrium separations are  $0.4$  Å longer than the gas phase-calculated distances (see Table 1) but are nevertheless consistent with a direct coordination of the ions with the benzene molecule.

A benzene molecule coming in direct contact with a hydrated ion results in the expulsion of a number of water molecules from the first solvation shell. For this reason small, strongly solvated ions, such as  $\text{Li}^+$  and  $\text{Na}^+$ , tend to retain their hydration structure and rarely associate with benzene. Figure 5b shows the number of water molecules in the first solvation shell of  $\text{Li}^+$ ,  $\text{Na}^+$ ,  $\text{K}^+$ , and  $\text{NH}_4^+$  as a function of the constrained CM separation between the ion and benzene ( $R_{MX}$ ). These coordination numbers are calculated from the pair distribution function  $g_{\text{MO}}$  up to the first minimum (2.56, 3.24, and 3.56 Å for  $\text{Li}^+$ ,  $\text{Na}^+$ , and  $\text{K}^+$ , respectively,<sup>46</sup> and 3.37 Å for  $\text{NH}_4^+$ ).

Figure 5b shows that the presence of a benzene molecule at distances from the ion near the gas phase equilibrium values (1.87, 2.43, 2.83, and 2.92 Å for  $\text{Li}^+$ ,  $\text{Na}^+$ ,  $\text{K}^+$ , and  $\text{NH}_4^+$ , respectively; see Table 1) results in significant loss of ion-coordinated water molecules. The high-energy shoulder of the PMF for lithium corresponds to the deformation of the tetrahedral coordination (at  $R_{MX} < 4.5$  Å) followed by the loss of one of the first-shell water molecules (at  $R_{MX} < 3.0$  Å). The shoulder for sodium corresponds to the loss of the loosely coordinated sixth water molecule from the first hydration shell (at  $R_{MX} < 6$  Å). Upon formation of a complex with benzene, potassium loses 1.6 water molecules, going from a coordination number of 6.9 in bulk water<sup>46</sup> to 5.3 at  $R_{MX} \sim 3.2$  Å. Ammonium loses only one water molecule, going from a coordination of 5.3 to 4.3 at  $R_{MX} \sim 3.3$  Å. This smaller loss of water molecules (compared to  $\text{K}^+$ ) is likely the reason why  $\text{NH}_4^+$  associates more strongly and over a longer range than  $\text{K}^+$ .

Although the QM and MM complexation energies of  $\text{Li}^+$  and  $\text{Na}^+$  with benzene (see Table 1) are underestimating the experimental enthalpies of formation of the complexes,<sup>10</sup> this does not

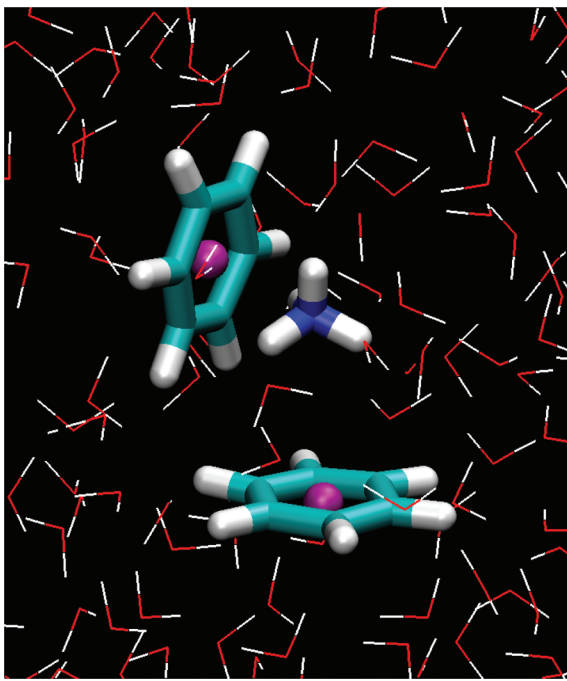


**Figure 6.** Snapshot of a representative configuration of the  $\text{NH}_4^+$ –(benzene)<sub>2</sub> complex in 600 SWM4-NDP water molecules. Atom colors are red for oxygen, blue for nitrogen, cyan for carbon, white for hydrogen, and pink for the nonatomic site of the benzene model.

affect the ion–benzene affinities in aqueous solution. Polarizable models optimized to reproduce the experimental binding energies of the complexes (−39.3 kcal/mol for  $\text{Li}^+$  and −22.5 kcal/mol for  $\text{Na}^+$ ) yield PMFs for the lithium–benzene and sodium–benzene pairs in solution that do not deviate from those of Figure 5 by more than 0.1 kcal/mol in the thermodynamically accessible region  $R_{\text{MX}} > 3 \text{ \AA}$  (data not shown).

Figure 5a also shows the PMF between the centers of two benzene molecules in water, displaying an equilibrium separation of 5.2 Å and a binding free energy of −1.1 kcal/mol, in excellent agreement with the value of  $-1.00 \pm 0.05$  kcal/mol for the heat of dimerization of benzene in water reported by Hallén et al.<sup>66</sup> This binding free energy of the benzene dimer in water represents an improvement over previous simulation results<sup>67–69</sup> which reported affinities are either too large (−1.5 kcal/mol for ref 67) or too small (−0.5 and −0.36 kcal/mol for refs 68 and 69, respectively).

**3.6. Effect of Cations on  $\pi$ – $\pi$  Interactions in Water.** The ab initio calculations reported in Table 1 show that an ion associating to a benzene dimer will form the more stable “ $\pi$ –cation– $\pi$ ” sandwich conformations in which two ring systems compete for a direct interaction with the cation, preferably to the less stable “cation– $\pi$ – $\pi$ ” conformation in which a cation and a ring system cooperate to bind a central ring system. In that regard, cation– $\pi$  interactions are disruptive to  $\pi$ – $\pi$  interactions in the gas phase. To reveal how the interplay between cation– $\pi$  and  $\pi$ – $\pi$  interactions translates in aqueous medium, we have performed MD simulations of two benzene molecules in water and two benzene molecules in presence of either one ammonium ion (see Figure 6) or one potassium ion.

The effect of the ion on the association of the two benzene molecules in water can be analyzed from the  $g_{\text{XX}}$  RDF, where X is benzene center, in presence and absence of the cation (see Figure 7a). The three curves are calculated from 100 ns

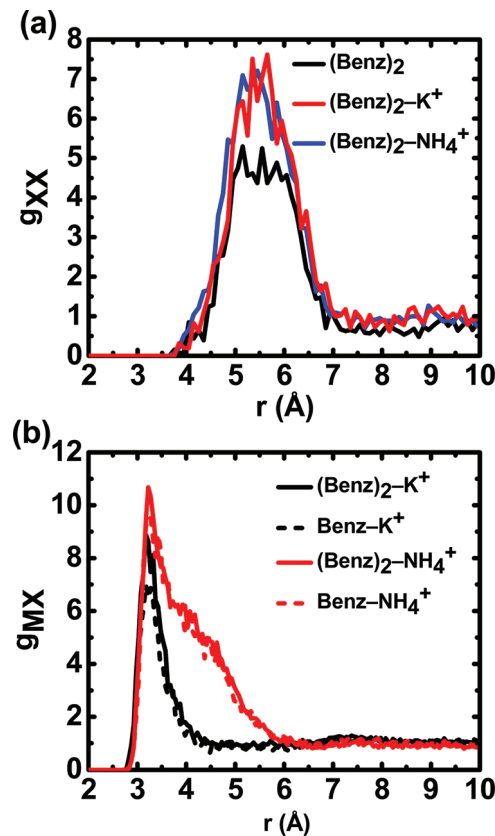


**Figure 7.** (a) Enhancement of the benzene–benzene radial distribution function ( $g_{\text{XX}}$ ) in the presence of a potassium or an ammonium ion. (b) Enhancement of the ion–benzene radial distribution function ( $g_{\text{MX}}$ ) in the presence of a second benzene molecule. Distributions obtained from 100 ns unconstrained simulations in 600 water molecules.

unconstrained simulations of the binary and ternary complexes and have similar shapes with a broad maximum in the range 5–6 Å. The function, however, possesses higher probability for the “ $\text{NH}_4^+$ ” and “ $\text{K}^+$ ” systems, indicating that  $\pi$ – $\pi$  association increases in presence of the cation.

The influence of the second benzene molecule on the cation– $\pi$  interaction can similarly be analyzed from the  $g_{\text{MX}}$  RDF, where M is  $\text{K}^+$  or N of  $\text{NH}_4^+$ . Figure 7b shows that the function, calculated from 100 ns unconstrained simulations, has a slightly higher probability for benzene–dimer complexes, compared to the monomer complexes. This indicates that cooperativity exists between cation– $\pi$  and  $\pi$ – $\pi$  interactions in aqueous solution.

The most probable arrangement of the two benzene molecules relative to the cation is investigated using 80 ns simulations in which an energy restraint is applied either to prevent the benzene centers of mass from separating by more than 7 Å or to prevent the cation and one benzene molecule from separating by more than 5 Å for  $\text{K}^+$  and 6 Å for  $\text{NH}_4^+$ . These biased simulations represent the interaction of the ion with a preformed benzene dimer and of the second benzene molecule with a preformed cation–benzene pair. A harmonic force constant of 5 kcal/mol/Å<sup>2</sup> is used for the restraints.

Figure 8a and c presents the distribution of the ion ( $\text{K}^+$  or  $\text{NH}_4^+$ ) as the conditional free energy surface  $-k_B T \ln[\rho_M(z_M, r_M)/2\pi r_M]$ , where  $\rho_M(z_M, r_M)$  is the ion density relative to the restrained benzene dimer, in cylindrical coordinates. The factor  $2\pi r$

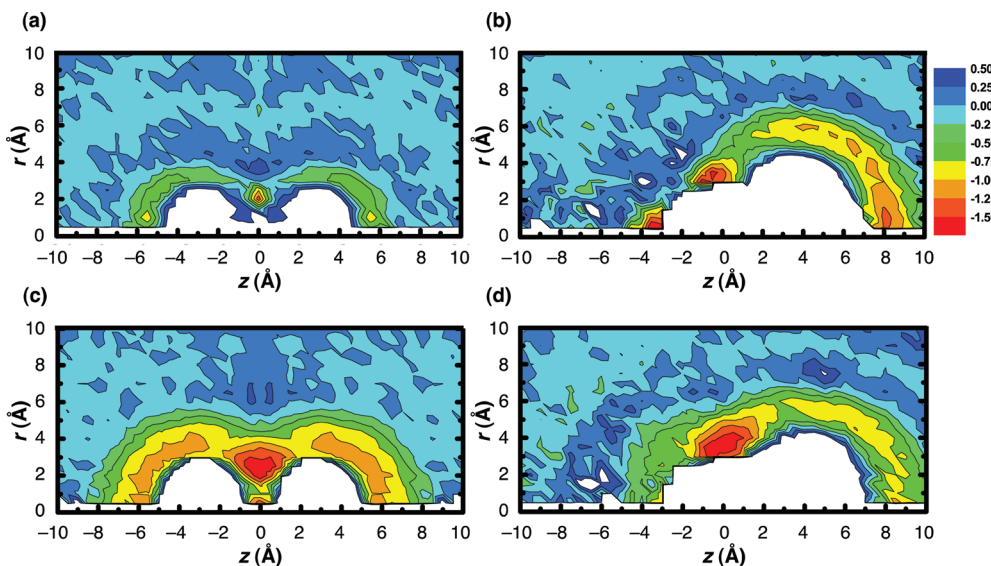


**Figure 8.** Distribution of (a)  $\text{K}^+$  around a preformed benzene dimer, (b) benzene around a preformed  $\text{K}^+$ –benzene pair, (c)  $\text{NH}_4^+$  around a preformed benzene dimer, and (d) benzene around a preformed  $\text{NH}_4^+$ –benzene pair. Densities are presented as the free energy surfaces  $-k_{\text{B}}T \ln[\rho(z,r)/2\pi r]$ , where  $\rho(z,r)$  is the distribution relative to the restrained solutes, in cylindrical coordinates. Benzene molecules are at  $z \sim \pm 2.7 \text{ \AA}$  and  $r = 0 \text{ \AA}$  in panels (a) and (c). In panels (b) and (d), the ion is at  $z = r = 0 \text{ \AA}$  and the benzene molecule is at  $z \sim 3.2 \text{ \AA}$  and  $r = 0 \text{ \AA}$ .

accounts for the purely geometric probability of finding the ion at a radial distance  $r$  from the benzene–benzene axis. Figure 8b and d shows function  $-k_{\text{B}}T \ln[\rho_X(z_X, r_X)/2\pi r_X]$ , the conditional free energy surface for a benzene molecule in the presence of a restrained ion–benzene dimer.

Figure 8a shows a high-density  $\text{K}^+$  “envelope” at a distance of 3.0–3.5 Å from either one of the two benzene molecules (which are located at  $z \sim \pm 2.6 \text{ \AA}$  and  $r = 0 \text{ \AA}$ ). This region corresponds to the minimum of the  $\text{K}^+$ –benzene PMF of Figure 5a. Maximum ion density is found at  $z = 0 \text{ \AA}$  and  $r \sim 2.0 \text{ \AA}$ , where the ion is coordinating both benzene molecules and forming an “isosceles triangle” conformation, and at  $z \sim 5.5 \text{ \AA}$  and  $r < 2 \text{ \AA}$ , where the system is forming a  $\text{K}^+$ –benzene–benzene stacked conformation.

Figure 8b shows a high-density benzene envelope at a distance of 5–6 Å from the ion-bound benzene molecule (located at  $z \sim 3.2 \text{ \AA}$  and  $r = 0 \text{ \AA}$ ) or at a distance of 3.0–3.5 Å from the  $\text{K}^+$  ion (located at  $z = r = 0 \text{ \AA}$ ). Three regions are markedly populated: the “triangle” conformation at  $z \sim 0 \text{ \AA}$  and  $r \sim 3.5 \text{ \AA}$ , the  $\text{K}^+$ –benzene–benzene stacked conformation at  $z \sim 8 \text{ \AA}$  and  $r < 2 \text{ \AA}$ , and the benzene– $\text{K}^+$ –benzene sandwich conformation at  $z \sim -3.5 \text{ \AA}$  and  $r < 1 \text{ \AA}$ . This sandwich conformation is not observed in Figure 8a due to the weak restraint on the benzene molecules, preventing them from separating. The “triangle” conformation is the most favorable arrangement and corresponds to a potassium ion coordinated by two benzene molecules forming an  $X \cdots M \cdots X \sim 90^\circ$  angle of  $\sim 90^\circ$ . Interestingly, the bent sandwich conformation, located between the “triangle” and sandwich conformations of Figure 8b, is poorly populated despite being the most stable structure in gas phase (see Table 1). This may be attributed to the higher degree of dehydration of the  $\text{K}^+$  ion accompanying this arrangement. Indeed, three additional simulations of the ternary complex with restraints keeping the  $X \cdots M$  distances within 3.2 Å and the  $X \cdots M \cdots X$  angle around  $90^\circ$ ,  $120^\circ$ , and  $180^\circ$  show that the  $\text{K}^+$  ion is coordinated by 4.1 water molecules for  $X \cdots M \cdots X \sim 90^\circ$ , 3.7 molecules for  $X \cdots M \cdots X \sim 120^\circ$ , and 4.1 molecules for  $X \cdots M \cdots X \sim 180^\circ$ . This shows that  $\text{K}^+$  is best hydrated when the complex adopts the “triangle” geometry

( $X \cdots M \cdots X \sim 90^\circ$ ) and poorly hydrated when it adopts the bent sandwich geometry ( $X \cdots M \cdots X \sim 120^\circ$ ). It also confirms that the “triangle” and straight sandwich arrangements are equally favorable, as both provide a solvation shell formed of two benzene and four water molecules.

The simulations involving  $\text{NH}_4^+$  display similar features (see Figure 8c and d) but with a marked preference for the triangle arrangement. The stacked and sandwiched geometries do not appear particularly favored or disfavored. Additional simulations with restraints keeping the  $X \cdots M$  distances below 3.3 Å, and the  $X \cdots M \cdots X$  angle at  $90^\circ$ ,  $120^\circ$ , and  $180^\circ$  shows that the  $\text{NH}_4^+$  ion is coordinated by 3.6 water molecules for  $X \cdots M \cdots X \sim 90^\circ$  and 3.3 water molecules for  $X \cdots M \cdots X$  angles of  $120^\circ$  and  $180^\circ$ . This confirms that the “triangle” conformation is the most favored and that straight and bent sandwich conformers are equally accessible.

#### 4. CONCLUSION

Ab initio calculations on cation– $\pi$  interactions of  $\text{Li}^+$ ,  $\text{Na}^+$ ,  $\text{K}^+$ , and  $\text{NH}_4^+$  with benzene show that cation– $\pi$  interactions in the gas phase become stronger if additional aromatic systems are introduced in stacked arrangements but weaker if they are introduced in sandwiched arrangements. The dominant contribution to this cooperativity effect is electronic polarization. Polarizable models are parametrized to reproduce the interactions of  $\text{Li}^+$ ,  $\text{Na}^+$ ,  $\text{K}^+$ , and  $\text{NH}_4^+$  with benzene as well as the interaction of  $\text{NH}_4^+$  with water. The models reproduce the ab initio energies of both the benzene complexes and the water complexes. The model for  $\text{NH}_4^+$  also reproduces the experimental hydration free energy of the ion without further adjustment.

Potentials of mean force between cation–benzene pairs in aqueous solution show that, while  $\text{Li}^+$  and  $\text{Na}^+$  do not bind benzene,  $\text{K}^+$  and  $\text{NH}_4^+$  bind with free energies of  $-1.2$  and  $-1.4 \text{ kcal/mol}$ , respectively. The small  $\text{Li}^+$  and  $\text{Na}^+$  ions form rigid complexes with their coordinating water molecules that cannot easily accommodate the replacement of a water molecule by a benzene molecule. The

larger  $K^+$  and  $NH_4^+$  ions, on the other hand, have more flexible hydration shells that are favorable to benzene inclusion.

Methyl substitution of ammonium hydrogens is reported to decrease the gas phase binding energy between the ions and benzene.<sup>19,70</sup> For example, while we report a binding energy of  $-17.58\text{ kcal/mol}$  between ammonium and benzene, Xu et al.<sup>19</sup> have reported a binding energy of  $-15.78\text{ kcal/mol}$  between methylammonium and benzene at the same level of theory and Felder et al.<sup>70</sup> have reported a binding energy of  $-8.40\text{ kcal/mol}$  between tetramethylammonium and benzene at the MP2/6-31G(d) level of theory. It would be interesting to use similarly derived polarizable models to investigate the enhanced hydrophobic association with benzene resulting from successive methylations of the ammonium ion.

The results provide new insight on the influence of inorganic salts on the solubility of aromatic hydrocarbons in water, the so-called “salting-out” effect.<sup>71,72</sup> The degree of salting-out for aromatic compounds depends on the salt in an apparently nonsystematic way. For benzene, the salting-out effect in presence of lithium, sodium, potassium, and ammonium chloride salts follows the order  $Na^+ > K^+ > Li^+ > NH_4^+$ .<sup>71</sup> Based on the binding free energies calculated in this work, we suggest that the salting-out effect follows two distinct mechanisms.  $Li^+$  and  $Na^+$ , which expel benzene molecules from their first hydration shells, are effectively decreasing the volume of solution available to benzene— $Na^+$  more so than  $Li^+$ , leading to benzene association and salting-out.<sup>73</sup>  $K^+$  and  $NH_4^+$  are also effectively decreasing the volume of solution available to benzene but according not only to their sizes (which are comparable) but also to their affinities for benzene. Since  $NH_4^+$  has a higher (and longer-range) affinity for benzene than  $K^+$ , the excluded volume it creates is smaller, and its salting-out effect is expected to be weaker. It is important to note, however, that the present explanation does not account for the counterion (e.g.,  $Cl^-$ ), which might play different roles in presence of different cations, as it was suggested for lithium chloride.<sup>74</sup>

While  $K^+-(benzene)_2$  and  $NH_4^+-(benzene)_2$  complexes in gas phase are significantly more stable in their sandwiched conformations than in their stacked conformations, the reverse is true in aqueous solution. The most stable arrangement of the two systems in water, however, corresponds to a “triangle” geometry in which the two benzene molecules are both directly coordinating the cation, at an angle of approximately  $90^\circ$ . This geometry preserves the benzene–benzene hydrophobic interaction, while minimizing ion dehydration.

The concepts put forward in the present work can be transposed to cation– $\pi$  interactions in proteins. While a single aromatic residue, such as phenylalanine or tryptophan, at the surface of a protein may not create enough binding affinity for  $K^+$  or  $NH_4^+$  ions to generate significant biological function, a binding site formed of multiple aromatic residues may.<sup>75–77</sup> Our simulations suggest that an L-shaped arrangement of two aromatic residues binds ions better than a stacked or sandwiched arrangement. This thermodynamic advantage may however not be a dominant driving factor in light of the fact that, unlike in solution, residues forming “aromatic cages” in proteins are likely to be preassembled and optimally oriented. Nevertheless, the fact that  $K^+$  and  $NH_4^+$  ions have different affinities for stacked and sandwiched arrangements of aromatic residues can possibly be exploited to design protein receptors selective to potassium or ammonium that rely more on selectively accommodating a partially hydrated ion than on providing a selective full coordination environment.<sup>78</sup>

The parametrization procedure introduced in this work can be readily applied to other aromatic moieties to provide a set of polarizable models representing the various cation– $\pi$  interactions found in proteins. Such models can likely help to elucidate the factors determining the abundances of the various cation– $\pi$  and cation– $\pi_2$  conformations surveyed in the Protein Data Bank<sup>79,80</sup> and can be used to study biological systems in which cation– $\pi$  interactions play important roles.

## ■ AUTHOR INFORMATION

### Corresponding Author

\*E-mail: guillaume.lamoureux@concordia.ca.

<sup>†</sup>On leave from Department of Chemistry, Faculty of Science, Assiut University, Assiut 71516, Egypt.

### Notes

The authors declare no competing financial interest.

## ■ ACKNOWLEDGMENT

This work was supported by an FQRNT Établissement de nouveaux chercheurs grant (NC-125413) and by a PROTEO scholarship to EAO. Computational resources were provided by the Réseau québécois de calcul de haute performance (RQCHP) and by an FQRNT Equipment grant.

## ■ REFERENCES

- (1) Dougherty, D. A. *Science* **1996**, *271*, 163–168.
- (2) Mecozzi, S.; West, A. P.; Dougherty, D. A. *J. Am. Chem. Soc.* **1996**, *118*, 2307–2308.
- (3) Mecozzi, S.; West, A. P.; Dougherty, D. A. *Proc. Natl. Acad. Sci. U.S.A.* **1996**, *93*, 10566–10571.
- (4) Ma, J. C.; Dougherty, D. A. *Chem. Rev.* **1997**, *97*, 1303–1324.
- (5) Gallivan, J. P.; Dougherty, D. A. *Proc. Natl. Acad. Sci. U.S.A.* **1999**, *96*, 9459–9464.
- (6) Woodin, R. L.; Beauchamp, J. L. *J. Am. Chem. Soc.* **1978**, *100*, 501–507.
- (7) Deakyne, C. A.; Meotner, M. *J. Am. Chem. Soc.* **1985**, *107*, 474–479.
- (8) Wouters, J. *Protein Sci.* **1998**, *7*, 2472–2475.
- (9) Armentrout, P. B.; Rodgers, M. T. *J. Phys. Chem. A* **2000**, *104*, 2238–2247.
- (10) Amicangelo, J. C.; Armentrout, P. B. *J. Phys. Chem. A* **2000**, *104*, 11420–11432.
- (11) Amunugama, R.; Rodgers, M. T. *J. Phys. Chem. A* **2002**, *106*, 5529–5539.
- (12) Ruan, C. H.; Rodgers, M. T. *J. Am. Chem. Soc.* **2004**, *126*, 14600–14610.
- (13) Yorita, H.; Otomo, K.; Hiramatsu, H.; Toyama, A.; Miura, T.; Takeuchi, H. *J. Am. Chem. Soc.* **2008**, *130*, 15266–15267.
- (14) Hallowita, N.; Carl, D. R.; Armentrout, P. B.; Rodgers, M. T. *J. Phys. Chem. A* **2008**, *112*, 7996–8008.
- (15) Caldwell, J. W.; Kollman, P. A. *J. Am. Chem. Soc.* **1995**, *117*, 4177–4178.
- (16) Cubero, E.; Luque, F. J.; Orozco, M. *Proc. Natl. Acad. Sci. U.S.A.* **1998**, *95*, 5976–5980.
- (17) Feller, D.; Dixon, D. A.; Nicholas, J. B. *J. Phys. Chem. A* **2000**, *104*, 11414–11419.
- (18) Tsuzuki, S.; Yoshida, M.; Uchimaru, T.; Mikami, M. *J. Phys. Chem. A* **2001**, *105*, 769–773.
- (19) Xu, Y.; Shen, J.; Zhu, W.; Luo, X.; Chen, K.; Jiang, H. *J. Phys. Chem. B* **2005**, *109*, 5945–5949.
- (20) Coletti, C.; Re, N. *J. Phys. Chem. A* **2006**, *110*, 6563–6570.

- (21) Frontera, A.; Quinonero, D.; Garau, C.; Costa, A.; Ballester, P.; Deya, P. M. *J. Phys. Chem. A* **2006**, *110*, 9307–9309.
- (22) Soteras, I.; Orozco, M.; Luque, F. *J. Phys. Chem. Chem. Phys.* **2008**, *10*, 2616–2624.
- (23) Mishra, B. K.; Bajpai, V. K.; Ramanathan, V.; Gadre, S. R.; Sathyamurthy, N. *Mol. Phys.* **2008**, *106*, 1557–1566.
- (24) Marshall, M. S.; Steele, R. P.; Thanthiriwatte, K. S.; Sherrill, C. D. *J. Phys. Chem. A* **2009**, *113*, 13628–13632.
- (25) Vijay, D.; Sastry, G. N. *Chem. Phys. Lett.* **2010**, *485*, 235–242.
- (26) Bernstein, F. C.; Koetzle, T. F.; Williams, G. J.; Meyer, E. F., Jr.; Brice, M. D.; Rodgers, J. R.; Kennard, O.; Shimanouchi, T.; Tasumi, M. *J. Mol. Biol.* **1977**, *112*, 535–542.
- (27) Minoux, H.; Chipot, C. *J. Am. Chem. Soc.* **1999**, *121*, 10366–10372.
- (28) Crowley, P. B.; Golovin, A. *Proteins: Struct. Funct. Bioinf.* **2005**, *59*, 231–239.
- (29) Wintjens, R.; Lievin, J.; Rooman, M.; Buisine, E. *J. Mol. Biol.* **2000**, *302*, 395–410.
- (30) Gromiha, M. M.; Santhosh, C.; Ahmad, S. *Int. J. Biolog. Macromol.* **2004**, *34*, 203–211.
- (31) Shi, Z. S.; Olson, C. A.; Kallenbach, N. R. *J. Am. Chem. Soc.* **2002**, *124*, 3284–3291.
- (32) Prajapati, R. S.; Sirajuddin, M.; Durani, V.; Sreramulu, S.; Varadarajan, R. *Biochemistry* **2006**, *45*, 15000–15010.
- (33) Lummis, S. C. R.; Beene, D. L.; Harrison, N. J.; Lester, H. A.; Dougherty, D. A. *Chem. Biol.* **2005**, *12*, 993–997.
- (34) Lehn, J.-M.; Meric, R.; Vigneron, J.-P.; Cesario, M.; Guilhem, J.; Pascard, C.; Asfari, Z.; Vicens, J. *Supramol. Chem.* **1995**, *5*, 97–103.
- (35) Archambault, F.; Chipot, C.; Soteras, I.; Luque, F. J.; Schulten, K.; Dehez, F. *J. Chem. Theory Comput.* **2009**, *5*, 3022–3031.
- (36) Sunner, J.; Nishizawa, K.; Kebarle, P. *J. Phys. Chem.* **1981**, *85*, 1814–1820.
- (37) Chipot, C.; Maigret, B.; Pearlman, D. A.; Kollman, P. A. *J. Am. Chem. Soc.* **1996**, *118*, 2998–3005.
- (38) Costanzo, F.; Della Valle, R. G.; Barone, V. *J. Phys. Chem. B* **2005**, *109*, 23016–23023.
- (39) Sa, R. J.; Zhu, W. L.; Shen, J. H.; Gong, Z.; Cheng, J. G.; Chen, K. X.; Jiang, H. L. *J. Phys. Chem. B* **2006**, *110*, 5094–5098.
- (40) (a) Drude, P. *Lehrbuch der Optik*; S. Hirzel: Leipzig, Germany, 1900. English translation: *The Theory of Optics*; Drude, P., translated from the German by Riborg Mann, C.; Millikan, R. A.; Dover Publications, Inc.: Mineola, New York, 1907.
- (41) Lamoureux, G.; Roux, B. *J. Chem. Phys.* **2003**, *119*, 3025–3039.
- (42) Anisimov, V. M.; Lamoureux, G.; Vorobyov, I. V.; Huang, N.; Roux, B.; MacKerell, A. D. *J. Chem. Theory Comput.* **2005**, *1*, 153–168.
- (43) Frisch, M. J. T., G. W.; Schlegel, H. B.; Scuseria, G. E.; Robb, M. A.; Cheeseman, J. R.; Scalmani, G.; Barone, V.; Mennucci, B.; Petersson, G. A.; Nakatsuji, H.; Caricato, M.; Li, X.; Hratchian, H. P.; Izmaylov, A. F.; Bloino, J.; Zheng, G.; Sonnenberg, J. L.; Hada, M.; Ehara, M.; Toyota, K.; Fukuda, R.; Hasegawa, J.; Ishida, M.; Nakajima, T.; Honda, Y.; Kitao, O.; Nakai, H.; Vreven, T.; Montgomery, J. A., Jr.; Peralta, J. E.; Ogliaro, F.; Bearpark, M.; Heyd, J. J.; Brothers, E.; Kudin, K. N.; Staroverov, V. N.; Kobayashi, R.; Normand, J.; Raghavachari, K.; Rendell, A.; Burant, J. C.; Iyengar, S. S.; Tomasi, J.; Cossi, M.; Rega, N.; Millam, N. J.; Klene, M.; Knox, J. E.; Cross, J. B.; Bakken, V.; Adamo, C.; Jaramillo, J.; Gomperts, R.; Stratmann, R. E.; Yazyev, O.; Austin, A. J.; Cammi, R.; Pomelli, C.; Ochterski, J. W.; Martin, R. L.; Morokuma, K.; Zakrzewski, V. G.; Voth, G. A.; Salvador, P.; Dannenberg, J. J.; Dapprich, S.; Daniels, A. D.; Farkas, O.; Foresman, J. B.; Ortiz, J. V.; Cioslowski, J.; Fox, D. J. *Gaussian 09*, revision B.01; Gaussian, Inc., Wallingford, CT, 2009.
- (44) Boys, S. F.; Bernardi, F. *Mol. Phys.* **1970**, *19*, 553–566.
- (45) Brooks, B. R.; Brooks, C. L.; Mackerell, A. D.; Nilsson, L.; Petrella, R. J.; Roux, B.; Won, Y.; Archontis, G.; Bartels, C.; Boresch, S.; Caflisch, A.; Caves, L.; Cui, Q.; Dinner, A. R.; Feig, M.; Fischer, S.; Gao, J.; Hodoscek, M.; Im, W.; Kuczera, K.; Lazaridis, T.; Ma, J.; Ovchinnikov, V.; Paci, E.; Pastor, R. W.; Post, C. B.; Pu, J. Z.; Schaefer, M.; Tidor, B.; Venable, R. M.; Woodcock, H. L.; Wu, X.; Yang, W.; York, D. M.; Karplus, M. *J. Comput. Chem.* **2009**, *30*, 1545–1614.
- (46) Yu, H. B.; Whitfield, T. W.; Harder, E.; Lamoureux, G.; Vorobyov, I.; Anisimov, V. M.; MacKerell, A. D.; Roux, B. *J. Chem. Theory Comput.* **2010**, *6*, 774–786.
- (47) MacKerell, A. D.; Bashford, D.; Bellott, M.; Dunbrack, R. L.; Evanseck, J. D.; Field, M. J.; Fischer, S.; Gao, J.; Guo, H.; Ha, S.; Joseph-McCarthy, D.; Kuchnir, L.; Kuczera, K.; Lau, F. T. K.; Mattos, C.; Michnick, S.; Ngo, T.; Nguyen, D. T.; Prodhom, B.; Reiher, W. E.; Roux, B.; Schlenkrich, M.; Smith, J. C.; Stote, R.; Straub, J.; Watanabe, M.; Wiorkiewicz-Kuczera, J.; Yin, D.; Karplus, M. *J. Phys. Chem. B* **1998**, *102*, 3586–3616.
- (48) Lamoureux, G.; Roux, B. *J. Phys. Chem. B* **2006**, *110*, 3308–3322.
- (49) Lopes, P. E. M.; Lamoureux, G.; Roux, B.; MacKerell, A. D. *J. Phys. Chem. B* **2007**, *111*, 2873–2885.
- (50) Ryckaert, J. P.; Ciccotti, G.; Berendsen, H. J. C. *J. Comput. Phys.* **1977**, *23*, 327–341.
- (51) Lamoureux, G.; Harder, E.; Vorobyov, I. V.; Roux, B.; MacKerell, A. D. *Chem. Phys. Lett.* **2006**, *418*, 245–249.
- (52) Essmann, U.; Perera, L.; Berkowitz, M. L.; Darden, T.; Lee, H.; Pedersen, L. G. *J. Chem. Phys.* **1995**, *103*, 8577–8593.
- (53) Lagüe, P.; Pastor, R. W.; Brooks, B. R. *J. Phys. Chem. B* **2004**, *108*, 363–368.
- (54) Kumar, S.; Bouzida, D.; Swendsen, R. H.; Kollman, P. A.; Rosenberg, J. M. *J. Comput. Chem.* **1992**, *13*, 1011–1021.
- (55) Souaille, M.; Roux, B. *Comput. Phys. Commun.* **2001**, *135*, 40–57.
- (56) Khavrutskii, I. V.; Dzubiella, J.; McCammon, J. A. *J. Chem. Phys.* **2008**, *128*, 044106.
- (57) Brugé, F.; Bernasconi, M.; Parrinello, M. *J. Chem. Phys.* **1999**, *110*, 4734–4736.
- (58) Brugé, F.; Bernasconi, M.; Parrinello, M. *J. Am. Chem. Soc.* **1999**, *121*, 10883–10888.
- (59) Klots, C. E. *J. Phys. Chem.* **1981**, *85*, 3585–3588.
- (60) Contreras, R.; Klopman, G. *Can. J. Chem.* **1985**, *63*, 1746–1749.
- (61) Åqvist, J. *J. Phys. Chem.* **1990**, *94*, 8021–8024.
- (62) Marcus, Y. *J. Chem. Soc., Faraday Trans.* **1991**, *87*, 2995–2999.
- (63) Tissandier, M. D.; Cowen, K. A.; Feng, W. Y.; Gundlach, E.; Cohen, M. H.; Earhart, A. D.; Coe, J. V.; Tuttle, T. R. *J. Phys. Chem. A* **1998**, *102*, 7787–7794.
- (64) Ben-Naim, A.; Marcus, Y. *J. Chem. Phys.* **1984**, *81*, 2016–2027.
- (65) Kumpf, R. A.; Dougherty, D. A. *Science* **1993**, *261*, 1708–1710.
- (66) Hallén, D.; Wadsö, I.; Wasserman, D. J.; Robert, C. H.; Gill, S. J. *J. Phys. Chem.* **1988**, *92*, 3623–3625.
- (67) Jorgensen, W. L.; Severance, D. L. *J. Am. Chem. Soc.* **1990**, *112*, 4768–4774.
- (68) Linse, P. *J. Am. Chem. Soc.* **1993**, *115*, 8793–8797.
- (69) Chipot, C.; Jaffe, R.; Maigret, B.; Pearlman, D. A.; Kollman, P. A. *J. Am. Chem. Soc.* **1996**, *118*, 11217–11224.
- (70) Felder, C.; Jiang, H.-L.; Zhu, W.-L.; Chen, K.-X.; Silman, I.; Botti, S. A.; Sussman, J. L. *J. Phys. Chem. A* **2001**, *105*, 1326–1333.
- (71) McDevit, W. F.; Long, F. A. *J. Am. Chem. Soc.* **1952**, *74*, 1773–1777.
- (72) Sanemasa, I.; Arakawa, S.; Araki, M.; Deguchi, D. *Bull. Chem. Soc. Jpn.* **1984**, *57*, 1539–1544.
- (73) Kalra, A.; Tugcu, N.; Cramer, S. M.; Garde, S. *J. Phys. Chem. B* **2001**, *105*, 6380–6386.
- (74) Thomas, A. S.; Elcock, A. H. *J. Am. Chem. Soc.* **2007**, *129*, 14887–14898.
- (75) Campagna-Slater, V.; Schapira, M. *Mol. Inf.* **2010**, *29*, 322–331.
- (76) Khademi, S.; O'Connell, J.; Remis, J.; Robles-Colmenares, Y.; Miercke, L. J.; Stroud, R. M. *Science* **2004**, *305*, 1587–1594.
- (77) Zheng, L.; Kostrewa, D.; Bernèche, S.; Winkler, F. K.; Li, X. D. *Proc. Natl. Acad. Sci. U.S.A.* **2004**, *101*, 17090–17095.
- (78) Chin, J.; Walsdorf, C.; Stranix, B.; Oh, J.; Chung, H. J.; Park, S.-M.; Kim, K. *Angew. Chem., Int. Ed.* **1999**, *38*, 2756–2759.
- (79) Reddy, A. S.; Vijay, D.; Sastry, G. M.; Sastry, G. N. *J. Phys. Chem. B* **2006**, *110*, 2479–2481.
- (80) Chelli, R.; Procacci, P. *J. Phys. Chem. B* **2006**, *110*, 10204–10205.